Chapter 5

Application of Ni-P Alloys to A Mold Material for Thermal Imprinting on Pyrex Glass

Harutaka Mekaru

Additional information is available at the end of the chapter

http://dx.doi.org/10.5772/60408

Abstract

The author developed a low-cost mold for imprinting on Pyrex glass. The mold was fabricated by the processing of micro-/nano-patterns made by FIB etching on an amorphous Ni-P alloy layer electroless-plated on Cu/Cr/Si, Ni/Ti/Si, and Inconel-600 substrates, followed by a thermal treatment, since a 400 °C for 3 h thermal treatment was known to increase the hardness of a Ni-P layer. The wt.% of P was changed to 4, 8, and 16; and scratch test and imprint experiments on the Pyrex glass showed Ni-16P/polished-Inconel-600 mold giving a best result. We also successfully demonstrated the making of line/space patterns, microlenses, and AIST logos on Pyrex glass. It was also experimentally proved that a Ni-P alloy can be used as a mold material to imprint on Pyrex glass at high temperature around 640 °C under vacuum without employing any release agent.

Keywords: Ni alloy, Thermal imprint, Hot embossing, Pyres glass, FIB, Microlens

1. Introduction

Nanoimprint lithography [1] has received considerable attention from the industry because it is capable of fabricating nanostructures at relatively low costs. Currently, UV-nanoimprint [2], [3] is beginning to make valuable contributions to the advancement of next-generation semiconductor manufacturing technology. In thermal nanoimprint [1], patterning on molds has been relatively difficult, especially when the application is related to optical components. In recent years, many applications of thermal nanoimprint technology to plastic and glass

materials have been developed [4]. In chemical and biochip devices, expensive disposable glass chips have largely been replaced by cheaper plastic chips. Plastic chips can be produced rapidly by mass production with molding techniques. However, glass chips are still used when the chips must be heated and cooled, or optical transparency demanded by high-resolution evaluation is required. Therefore, we are developing micro- and nanoimprint lithography technology for glass. A glass-nanoimprint lithography experiment was carried out, and the author succeeded in molding line and space patterns with linewidths of 300 nm on Pyrex glass (glass transition temperature T_g=560 °C) and quartz (T_g=1300 °C) [5], [6]; and an original thermal nanoimprint system was also developed [7], [8]. Moreover, a diamond mold for specializing in the imprinting on Pyrex glass was also developed [9]. However, the manufacturing application of this technique might not go far because the materials used here, such as glass-like carbon (GC) mold, and the diamond mold are expensive. In these glass-nanoimprint lithography experiments, GC that was selected as the mold material is still stable at a temperature of 1650 °C. However, there remain some problems when GC is used industrially as a mold material. GC is an expensive material, and is difficult to machine because of its fragility. Moreover, GC is brittle and it cannot withstand pressures of over 5.23 MPa [10]. As a result, it is quite difficult to make molds with high-aspect-ratio patterns.

2. Ni-P/Cu/Cr/Si mold

The fabrication technology of metallic micro - and nanostructures by plating is widely used in the manufacturing of wiring for electronic devices, the processing of optical components, and chemical and biochip devices. An electroformed Ni is often chosen as a material for metallic molds used for thermal nanoimprint lithography of engineering plastics such as polymethyl acrylate and polycarbonates because the extraction process is rapid and its machining is easy. Moreover, electroformed Ni is suitable for molding with high loads because the mechanical strength on Ni significantly improved after alloying. For glass nanoimprint technology, widely employed in the industry, the development of comparatively inexpensive Ni alloy molds like Ni-P [11], [12] and Ni-W [13] has resulted in significant advancements in the area. After searching through many Ni alloys [14], [15], [16], we chose an amorphous Ni-P alloy to serve as mold material for our work. The rationale behind this choice was the ease of working with the amorphous material, and that its mechanical characteristics improve with thermal treatment. In addition, when a nanopattern is formed on a curved surface such as, on a cylinder mold used with roller nanoimprint lithography [17], electroformed Ni–P alloy is selected in a great majority of cases. So we thought of making the Ni alloy as amorphous, and then use it as a mold for Pyrex-glass nanoimprint lithography.

2.1. Fabrication and patterning

In an amorphous material, the atomic arrangement is roughly in a thermodynamically metastable state. A lot of amorphous metals are employed in alloy plating with metals that can usually plate nonmetals or high-melting point metals. In these alloy-plating methods, the size

http://dx.doi.org/10.5772/60408

of the crystal becomes smaller as the proportion of the secondary element increases. The entire film adopts an amorphous structure with a sufficient content of a secondary element [18]. As a mold material, we chose to use the amorphous Ni–P alloy in conjunction with an electroless-plating method because it allows easy fabrication. For this experiment, 4-inch Si wafers were used for substrates on which a chrome layer of 0.1 μm thickness was formed by sputtering for adhesion-force improvement. Then a copper layer of 1 μm thickness was deposited on it by sputtering as a seed layer. Next an amorphous Ni–P alloy layer of 10 μm thickness was formed on this substrate. Table 1 shows the optimum conditions for electroless-plating with amorphous Ni–P alloy and for electroplating with pure Ni, which was used for a comparison. The determination that the Ni–P alloy was, in fact, amorphous, was made using the measurement results from X-ray diffraction. Figure 1 shows an X-ray-diffraction spectra of electroplated pure Ni layer and electroless-plated Ni–P alloy. The X-ray-diffraction peaks of fcc Ni(111) and Ni(200) observed in the pure Ni layer is broad, and an amorphous halo peak can be observed in the Ni–P alloy. The intensity of the Ni(111) diffraction line decreases gradually as the content of P increases in the Ni–P alloy. When the content of P becomes 11 wt.% or more, a broad spectrum, which is peculiar to amorphous materials [11], is observed. Therefore, we concluded that the electroless-plated Ni–P alloy (with a content of P=8 wt.%) was sufficiently amorphous. The mold pattern was etched with focused-ion-beam (FIB) lithography. The FIB system used in this experiment was an FB-2000A from the Hitachi High-Technologies Corporation. We drew the pattern by using an aperture of 100 μm diameter, in consideration of a trade-off between the processing speed and the accuracy of the pattern. Figure 2 shows the processing speed for Si, pure Ni, and amorphous Ni-P alloy. The total ion-beam charge irradiated to an area of 1 μm^2 square was calculated according to this procedure. This value was plotted against the horizontal axis. The process depth produced by FIB for each substrate was measured by using a three-dimensional (3D) optical profiler NewView 5000 (Zygo); and was plotted against the vertical axis. In the result, the processing speed using FIB with amorphous Ni-P alloy was found to be almost same as that with the Si. In addition, a remarkable difference appears between the pure Ni and the amorphous Ni-P alloy in relation to the process accuracy. Figure 3(a) is a scanning-electron microscope (SEM) image of line and space patterns with linewidths of 500 nm and 1 μm made on a pure Ni substrate using FIB with an irradiated-ion-beam charge of 80 $\mu C/\mu m^2$. A Hitachi S-3000H SEM was used for the observations. The insertion figure is an expanded SEM image of the line and space patterns observed from a vertical direction at a depression angle of 30°. The processed surface was very rough, and the crystal grain seemed to have worsened the FIB etching considerably. The crystal size of the pure Ni layer was measured by a transmission electron microscope (TEM). The maximum crystal size was 500 nm. On the other hand, in processing the amorphous Ni-P alloy shown in Fig. 3(b), high process accuracy was achieved, and the surface was very smooth after etching under the same condition as in the case of the pure Ni. It would seem that when the pattern size is smaller than the size of the crystal grains used in the mold material, utilizing an amorphous material is effective, and improves the process accuracy.an aperture of 100 μm diameter, in consideration of the balance between the processing

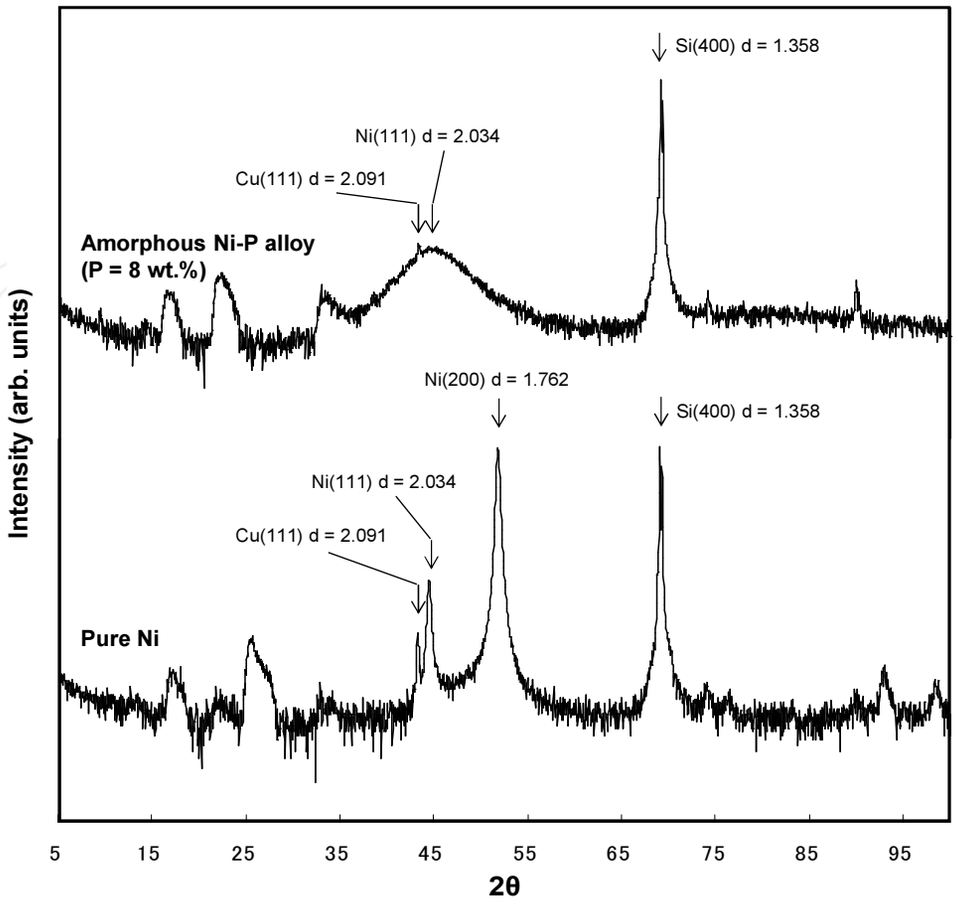

Figure 1. X-ray-diffraction spectra of electroplated pure Ni and electroless-plated Ni-P alloy.

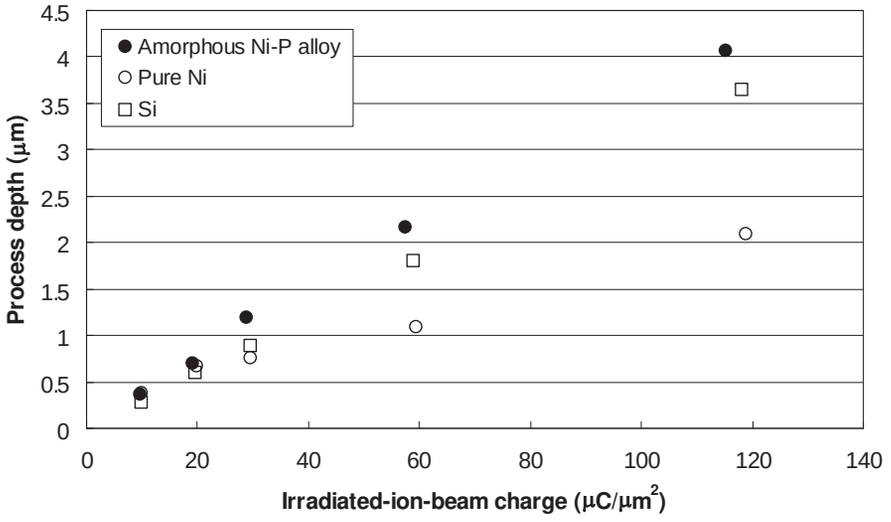

Figure 2. Relation between irradiated-ion-beam charge and process depth of Si, electroplated pure Ni, and electroless-plated Ni-P alloy.

http://dx.doi.org/10.5772/60408

	Ni-P electroless plating	**Ni electroplating**
Content ratio of P	8 wt.%	0 wt.%
Substrate	Cu/Cr/Si, Ni/Ti/Si,	Ni/Ti/Si
Degreasing	ACE CLEAN A-220*: 30 g/L Temperature: 50° C Time: 1 min	OPC CLEAN 91*: 8 ml /L Temperature: 23° C Time: 1 min
Activation	ICP ACCERA*: 200 ml/L Temperature: 25° C Time: 1 min	
Plating	TOP NICORON NAC-A*: 80 ml/L + TOP NICORON NAC-B*: 200 ml/L Temperature: 90° C Time: 50 min	Sulfamine acid nickel: 600 g/L Temperature: 50° C Time: 200 min Current density: 500 A/m^2
Washing	Distilled water Temperature: 25° C	Distilled water Temperature: 23° C

* Product of Okuno Chemical Industries Co., Ltd.

Table 1. Plating conditions of amorphous Ni-P alloy and pure Ni.

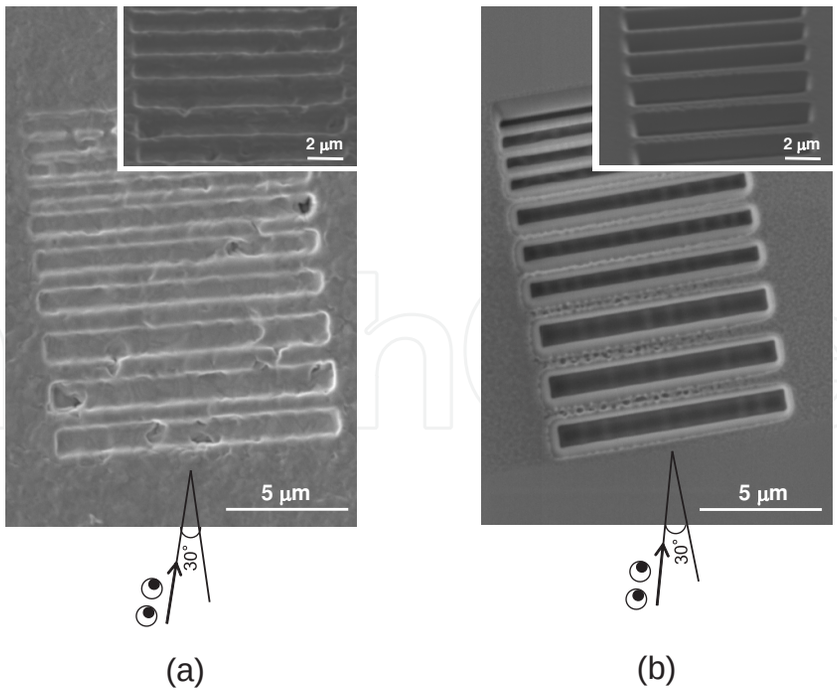

Figure 3. SEM images of patterns etched by FIB on: (a) electroplated pure Ni, and (b) the electroless-plated Ni-P alloy. Expanded SEM images, from a vertical direction, of line and space patterns at a depression angle of 30°.

2.2. Thermal nanoimprint system and experimental procedure

Figure 4 shows a photograph and specifications of a high-temperature thermal nanoimprint system ASHE0201 [7] (Engineering System) used for the glass-nanoimprint lithography experiment. To apply the mold on to a Pyrex glass at high temperature two ceramic loading stages (upper and lower) were employed. To experiment at a high temperature, the upper and bottom stages were made from ϕ90 mm ceramic plates. The backs of the loading stages were fitted with graphite heaters and cooling devices where the later were connected to a chiller system. The graphite heater and a cooling system were built into the back of the ceramic plates. A mold could be heated up to 1400 °C in this system. This system had a vacuum chamber of the bellow's type. When the setup was completed the bellows-type chamber was closed, and then the molecular turbo pump was started following a rotary pump. The loading stages could be decompressed to 0.07 Pa with a rotary pump and a turbo molecular pump. A load of 4.9 kN or less was applied with a servomotor. Figure 5 shows the sample setup and procedure for the thermal imprint experiment. The sequence of the experiment was:

1. The starting point of the upper loading stage drive was detected.
2. A 2-mm-thick GC sheet was put on the bottom loading stage for leveling adjustments.

To fix this sheet, thick GC blocks were arranged.

3. With its pattern side up, an amorphous Ni-P alloy mold was put on the lower stage.
4. A 0.5-mm-thick Pyrex glass was put on top of the amorphous Ni-P mold.
5. Another 2-mm-thick GC sheet was put on top of thnume Pyrex glass.

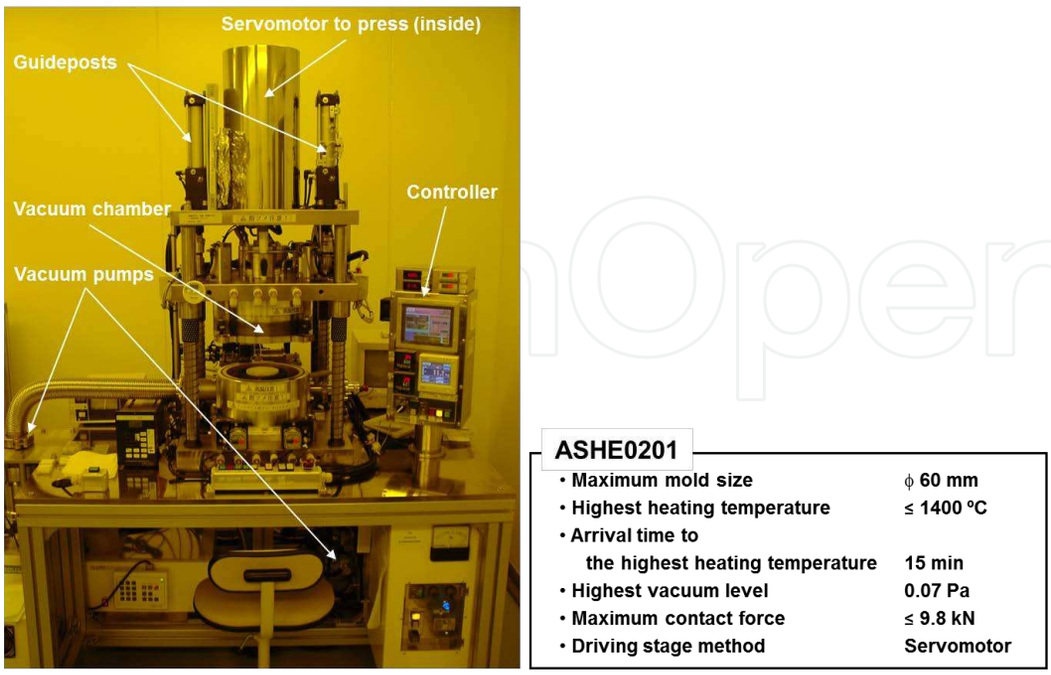

Figure 4. Photograph and specifications of the high-temperature thermal nanoimprint system used.

http://dx.doi.org/10.5772/60408

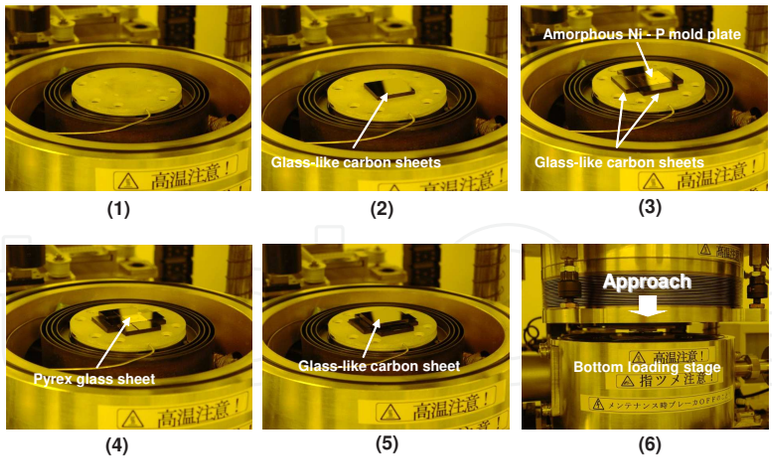

Figure 5. Setup procedure for an amorphous Ni-P alloy mold and Pyrex glass in the high-temperature thermal nano-imprint system.

6. The upper stage was lowered and brought close to the GC sheet until the space between the two was 1 mm or less.
7. The bellow's-type chamber was closed when the setup of the sample was completed; and then the molecular turbo pump was started following the rotary pump.
8. When the pressure in the chamber reached 10 Pa or less, the switches of the graphite heaters mounted on the upper and lower stages were turned on.
9. When the temperature reached a set value, a contact force was applied and maintained for a fixed time.
10. Afterwards, the cooling process was started, and we waited for the amorphous Ni-P mold and Pyrex glass to cool down to 150-200 ^{0}C in the vacuum for about 1 h.
11. The vacuum pump was stopped; the chamber was vented out to the atmosphere, and the upper stage was raised completely.
12. The Ni-P mold and Pyrex glass (adhered to each other) were removed from the chamber and manually pulled apart.

2.3. Experimental results and discussion

Line and space patterns with a depth of 3 μm and linewidths of 500 nm, 750 nm, and 1 μm were produced on an amorphous Ni-P alloy by FIB. After the FIB etching, the amorphous Ni-P alloy was thermally treated for 3 h at 400 °C by using the high-temperature thermal nano-imprint system ASHE0201. The Vickers hardness of the amorphous Ni-P alloy was increased to HV=873 by thermally treating it at 400 °C. In addition, the hardness of the amorphous Ni-P alloy was HV=1048, which is about 4.4 times that of the pure Ni when heated up to 600 °C, which is the molding temperature of the Pyrex glass. Moreover, the transformation of the pattern by thermal treatment was investigated. The SEM images of the line and space patterns before and after the thermal treatment are shown in Fig. 6.

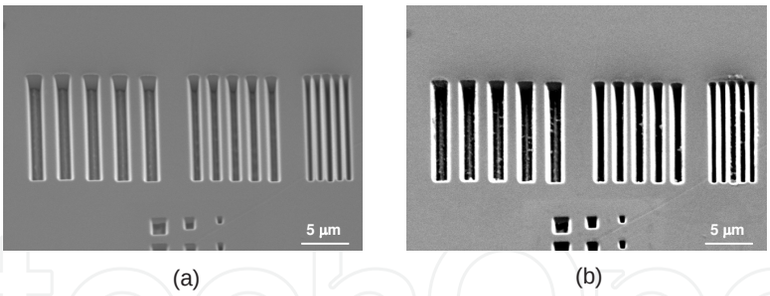

Figure 6. SEM images of line and space patterns on an amorphous Ni-P alloy mold (a) before and (b) after thermal treatment at 400 °C.

Molding conditions in this experiment were: heating temperature of 600 °C, maximum contact force of 5 kN, and contact time of 10 or 20 min. (The influence of the contact time on the molding accuracy was later investigated.) Subsequently, the graphite heaters were turned off and the amorphous Ni-P alloy mold and the Pyrex glass (Iwaki glass, Tg = 560 ºC) were let to cool down to 150 °C in the vacuum chamber. For contact times of 10 and 20 min, the SEM images of the line and space patterns on the Pyrex glass are shown in Figs. 7(a) and 7(b), respectively. Moreover, cross-sectional profiles are shown by the white lines in the SEM images, measured with an atomic-force microscope (AFM) SPA-501 (SII NanoTechnology). We achieved the molding line and space patterns with linewidths of 750 nm and 1 μm. Because the heating temperatures were a little low, the Pyrex glass was not completely filled into the mold patterns. Therefore, the surface of the imprinted patterns curved and a clear profile could not be measured. The pattern produced using a 20 min contact time was higher than that for 10 min, although the height of the pattern was less than 3 μm. No variation was observed in the shape of the molding pattern even though the experiment was repeated ten times or more under various molding conditions.

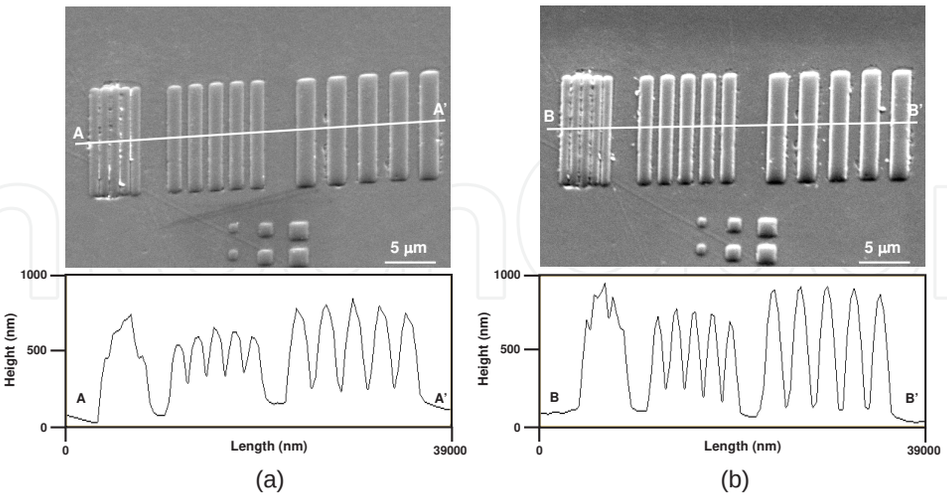

Reprinted with permission from Journal of Vacuum Science & Technology A 2007; 25(4) 1025-1028. Copyright 2007 American Vacuum Society.[19]

Figure 7. SEM and cross-sectional AFM images of line and space patterns on Pyrex glass after thermal imprint at contact times of: (a) 10 and (b) 20 min.

http://dx.doi.org/10.5772/60408

3. Ni-P/Ni/Ti/Si molds

In the process of fabricating a low-cost Ni-P alloy mold, an amorphous Ni-P plating layer on a silicon substrate was formed employing electroless-plating. However, prior to this plating, a 100-nm-thick Cr film was deposited on a silicon substrate to serve as an interlayer, and the deposited Cr film was then coated with a 1-μm-thick Cu film to serve as a seed layer to initiate the plating process. The electroless-plating resulted in the formation of a10-μm-thick Ni-P alloy layer on top of the Cu layer. Then, by the help of FIB etching, sets of line and space patterns were created on the Ni-P layer. The mold thus made, was used for thermal imprinting on a Pyrex glass [19]. In this thermal naoimprint work, however, the allowable heating temperature was only up to 600 ^{0}C. With this restriction the transcription shape of the imprinted patterns on a Pyrex glass turned out to be less than desirable. When the temperature was raised up to of 620 ^{0}C, the Ni-P alloy layer began to flake off from the Si substrate. It is believed that this phenomenon was caused by poor adhesive property of the Cr layer. The author then looked into other materials for the job. We used 500-nm-thick nickel layer as a seed layer and a 10-nm-thick Titanium layer as an interlayer that was sputter deposited on a 400-μm-thick Si wafer. Ti was used as an interlayer, because it has been known to increase the adhesive force by its anchoring properties.

3.1. Fabrication and patterning

For the purpose of comparison with an earlier work using the Cu/Cr/Si substrate [19], here the P content was set to 8 wt.%. Moreover, an electroplated layer of pure Ni on a Ni/Ti/Si substrate was also prepared for the purpose of comparison. Table 1 shows the parameters used for the various plating processes involved in these experiments. The mold pattern was created using FIB lithography that employed an EIP-5400 system (Elionix). Here, an ion-beam from a liquid Ga metallic ion source was accelerated by 40 kV to irradiate the surface of the sample. The beam current during the FIB processing was 0.5 nA. The FIB system was equipped with an improved version of the original 3D computer-aided-design (CAD) software. With this software, it was possible to process each layer by resolving 3D shape. The mold pattern in shape of microlenses were created as FIB scanned the concentric circle into which the multi-layer was divided. The etch times for the microlens pattern of curvature radii 12 μm and 20 μm were 113 min and 53 min, respectively. Figures 8(a) and 8(b) show SEM images of the microlens pattern in the curvature radii of 12 μm and 20 μm that were etched into the pure Ni substrate using FIB. Figures 8(c) and 8(d) show SEM images of the microlens pattern in the curvature radii of 12 μm and 20 μm etched into the amorphous Ni-P alloy substrate using FIB.

3.2. Experimental results and discussion

For the thermal imprint on Pyrex glass experiments a high-temperature thermal nanoimprint system ASHE0201 was used. When the temperature of the stage reached 620 ^{0}C, a contact force of 1 kN was then applied to the upper stage and was maintained there for 10 min. Afterwards, the mold and the Pyrex glass were cooled down to 200 ^{0}C, while still under vacuum. No release agent of any kind was used in the experiment. Figures 9(a) and 9(b) are the SEM images of the microlenses with the curvature radii of 12 μm and 20 μm imprinted on a Pyrex glass Pyrex

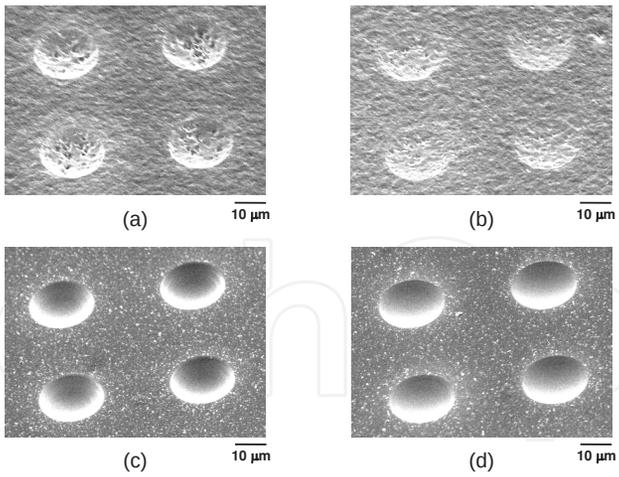

Figure 8. SEM image of a mold pattern of microlenses with the curvature radii of: (a) 12 and (b) 20 μm on the pure Ni mold. SEM image of a mold pattern for microlenses with the curvature radii of: (c) 12 and (d) 20 μm on the amorphous Ni-P alloy mold.

glass by using pure Ni mold. However, in Fig. 9(b) an imprinted microlens could not be observed. This could be related to the microlens pattern becoming indistinguishable in the noisy background of the rough surface. The surface roughness is an important factor in the fabrication of microlenses, especially because processing accuracy on pure Ni has been known to be poor. The irregularity of the surface of the pure Ni mold was transcribed on the Pyrex glass by the influence of the crystal grains on the mold surface. Figures 9(c) and 9(d) are SEM images of microlenses with the curvature radii of 12 μm and 20 μm imprinted on a Pyrex glass by using the amorphous Ni-P alloy mold. The imprinted patterns on a Pyrex glass lens were very smooth as shown in Figs. 9(c) and 9(d), their difference from the pure Ni mold is quite apparent.

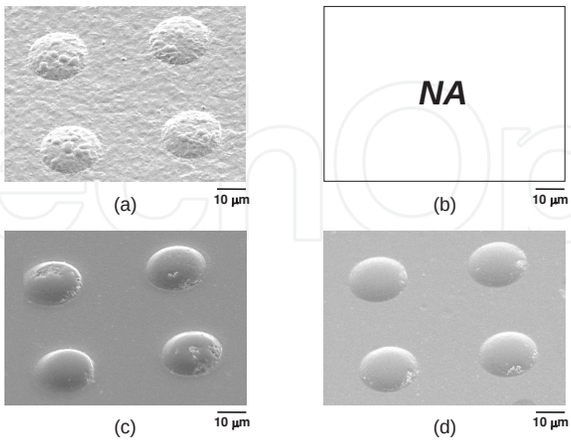

Reprinted from Microelectronic Engineering 2012; 85 873-876. [20]

Figure 9. SEM images of imprinted microlenses with the curvature radii of: (a) 12 and (b) 20 μm on a Pyrex glass using pure Ni mold. SEM images of imprinted microlenses with the curvature radii of: (c) 12 and (d) 20 μm on a Pyrex glass using the amorphous Ni-P alloy mold.

http://dx.doi.org/10.5772/60408

4. Ni-P/Inconel alloy molds

In previous experiments, the amorphous Ni-P alloy layer was electroless-plated on a Si substrate previously sputter-deposited with a 100-nm-thick interlayer of Cr and a 1-μm-thick seed layer of Cu [19]. However, the Ni-P/Cu/Cr/Si mold had weak adhesion forces between its different layers, and their maximum heat-proof temperature was only 600ºC. To address this difficulty, the interlayer was changed to a 10-nm-thick Ti layer, and the seed layer was changed to a 500-nm-thick Ni layer. Thus the mold composed of Ni-P/Ni/Ti/Si layers could then be used to imprint Pyrex glass at a higher temperature of 630 ºC [20]. However, from the imprinting experiments on Pyrex glass it appeared that the heating temperature would need to be 630-640 ºC. However, molds capable of functioning at even higher temperatures up to 650 ºC were considered more desirable. Therefore, we changed the substrate material from Si to Inconel-600.

4.1. Fabrication of molds

4.1.1. Electroless-plating

The author thought that the electroless-plated Ni-P alloy layer flaked off the Si substrate because the adhesion forces with the Cr layer were insufficient. We, therefore, changed the material. A 500-nm-thick Ni layer as a seed layer and a 10-nm-thick Ti interlayer were sputter-deposited on a 400-μm-thick Si. Ti was used because, as an interlayer, it increases the adhesion forces by an anchoring effect. The amorphous Ni-P alloy layer was deposited on the substrate by electroless-plating. For this case, the Ni-P alloy layer was deposited under three different plating conditions such that the content ratios of P could be set at 4, 8, and 16 wt.%. Details of each plating process are summarized in Table 2. The purpose of working with the three kinds of molds was to investigate the influence of the content ratios of P on the characteristics of the mold material. Moreover, an electroplated layer of pure Ni on a Si substrate fabricated under the same conditions as in Table 1 was also prepared to compare the X-ray diffraction data. In this section, the Ni-P alloy layers with content ratios of 4, 8, and 16 wt.% are labeled Ni-4P, Ni-8P, and Ni-16P. After plating, the substrate was diced into small square pieces of sides 30 mm in size; these pieces were thermally treated in a preliminary experiment. Each substrate was heated to 400 ºC for 3 h. Cross-sectional SEM images of the mold substrates of Ni-4P, Ni-8P, and Ni-16P are shown in Figs. 10(a), 10(b), and 10(c). Flaking-off of the plated layer was observed in all types of substrates. The Ni-P plated layer had flaked off from the Ni seed layer and the Ti interlayer in the Ni-4P/Ni/Ti/Si substrate. In the higher P density substrate, the bulk Si of the Si substrate cracked and flaked off while still adhering to the Ni-P plated layer. It appeared that the Ni-P plated layer had flaked off to relieve some internal stress developed during the thermal treatment because of some mismatch in the coefficients of thermal expansion of the two materials (Ni: 17:2 x 10^{-6}/K, Si: 4:4 x 10^{-6}/K, at 1000 K) [21]. We changed the substrate material from Si to Inconel-600 because Inconel-600 is a Ni alloy composed of 72% Ni (+Co), 14–17% Cr, 6–10% Fe [22] and the coefficient of thermal expansion of Inconel-600 (15.8 x 10^{-6}/K, at 973 K [21]) is almost equal to that of the bulk Ni. The size of the Inconel-600 substrate was 30 x 30 x 0.5 mm^3. To investigate the effect of chemical-mechanical polishing

(CMP) on the Inconel-600 substrate before the electroless-plating of the Ni-P layer, two kinds of Inconel-600 substrates were prepared. One was polished to a surface roughness of 10 nm while the other was left unpolished. Then, a 10-μm-thick Ni-P plated layer was deposited on the Si and Inconel-600 substrates under the plating condition described in Table 2. To evaluate the sticking power between the Ni-P layer and the substrate, a scratch test was done with tweezers and repeated ten times; results of this test are shown in Fig. 11.

Content ratio of P	**4 wt.%**	**8 wt.%**	**16 wt.%**
Substrate	Ni/Ti/Si, Inconel 600	Ni/Ti/Si, Inconel 600	Ni/Ti/Si, Inconel 600
Degreasing	Sodium hydroxide 15 g/L Sodium silicate, ortho 30 g/L Sodium alkylbenzene sulfonate 0.1 g/L Temperature: 23 °C Time: 40 s	Dipsol AL-45b) 40 g/L Temperature: 50 °C Time: 3 min	Sodium hydroxide 15 g/L Sodium silicate, ortho 30 g/L Sodium alkylbenzene sulfonate 0.1 g/L Temperature: 23 °C Time: 40 s
Activation	19.93% HCl Temperature: 23 °C Time: 8 min	HCL : 500 mL/L Temperature: RT Time: 0.5 min NiCl strike plating Temperature: 35 °C Time: 4 min	19.93%HCl Temperature: 23 °C Time: 8 min
Electroless plating	Sumer S-795 a) Temperature: 90 °C Time: 60 min	Dipsol NP-1900 b) Temperature: 88 °C Time: 40 min	Sumer S-795 a) Temperature: 90 °C Time: 60 min
Washing	Distilled water Temperature: 23 °C	Distilled water Temperature: RT	Distilled water Temperature: 23 °C

a) Product of JAPAN KANIGEN Co., Ltd.

b) Product of Dipsol Chemicals Co., Ltd.

Table 2. Electroless-plating conditions of amorphous Ni-P alloy.

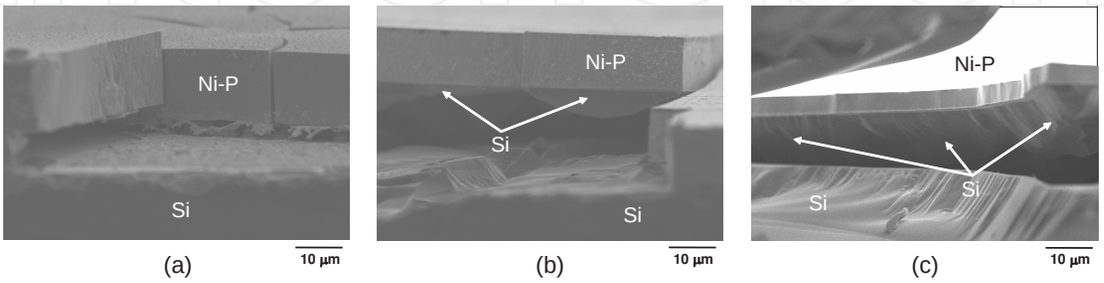

Figure 10. Cross-sectional SEM images of electroless-plated Ni-P alloys that flaked off from the Si substrate after heating at 400 ºC. Content ratio of P: (a) 4, (b) 8, and (c) 16 wt %.

http://dx.doi.org/10.5772/60408

As can be seen from this figure, a Ni-8P/unpolished-Inconel-600 substrate was not fabricated for these tests. The flaking off phenomenon by scratching was not observed in every substrate, although some black spots were observed on the Ni-4P/unpolished-Inconel-600 substrate. In the next step in this experiment, other substrates were thermally treated under the following conditions and sequence: first, the plated substrates were treated thermally at 400 ºC for 3 h. After that, they were heated at 650 ºC for 10 min. The substrates were then left to cool down to room temperature. Then 10 scratch examinations were executed. The Ni-P alloys electroless-plated on a Si substrate flaked off completely as shown in Fig. 12. The Ni-16P layer flaked off from the Si substrate completely even before scratching. This behavior was thought to be caused by the difference in the coefficients of thermal expansion of the Ni-P plated layer and the Si substrate as mentioned earlier. On the other hand, when the Inconel-600 substrate was used, Ni-P plated layers remained firmly adhered to the Inconel-600 substrate.

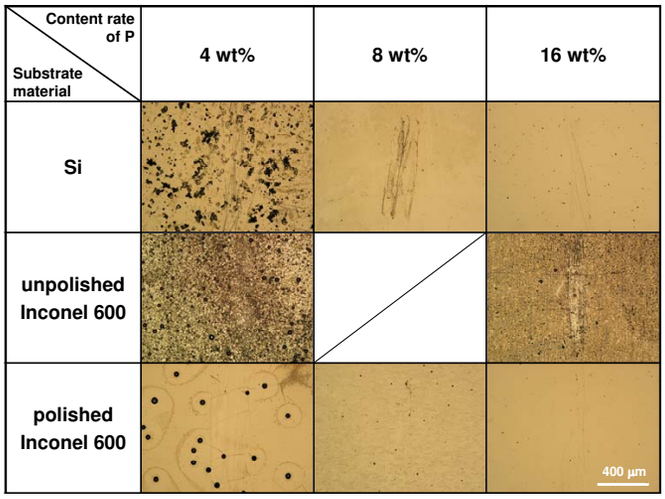

Figure 11. Results of scratch test on Ni-P alloy layers before thermal treatments.

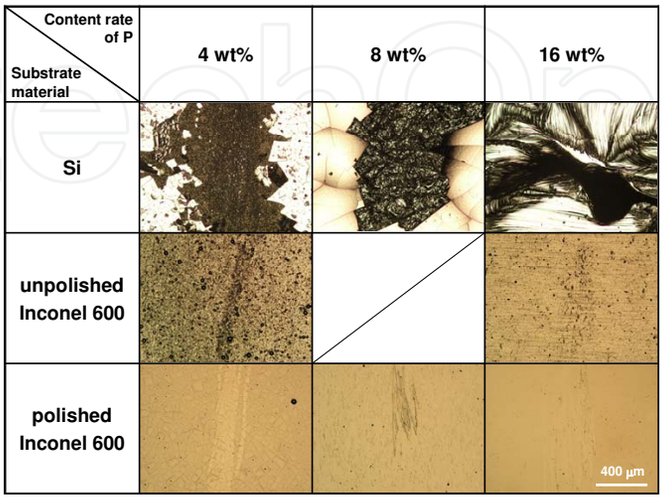

Figure 12. Results of scratch test of Ni-P alloy layers after thermal treatments.

4.1.2. Etching using FIB

A mold pattern was processed with FIB lithography using EIP-5400 system. FIB etching was performed under the same conditions that processed microlenses as shown in Fig. 8. Figure 13 shows the SEM images of the microlens pattern with the curvature radii of 12 and 20 μm etched with FIB on the Ni-P/Inconel-600 substrates before CMP. The image shows that the surface of the Ni-P layer was very uneven, and there were swellings of the same size as of the microlens pattern on the Ni-4P/unpolished-Inconel-600 substrate. This roughness seemed to originate from the surface roughness of the unpolished Inconel-600 substrate. Figure 14 shows the microlens pattern etched by FIB on the Ni-4P/polished Inconel-600 substrate. In this substrate, cracks were seen, and a part of the microlens pattern was affected. On the other hand, on the polished Inconel-600 substrate electroless-plated by Ni-8P and Ni-16P, the microlens pattern had a very smooth surface. From these results, Ni-4P/Inconel-600 seemed to be unsuitable for mold material.

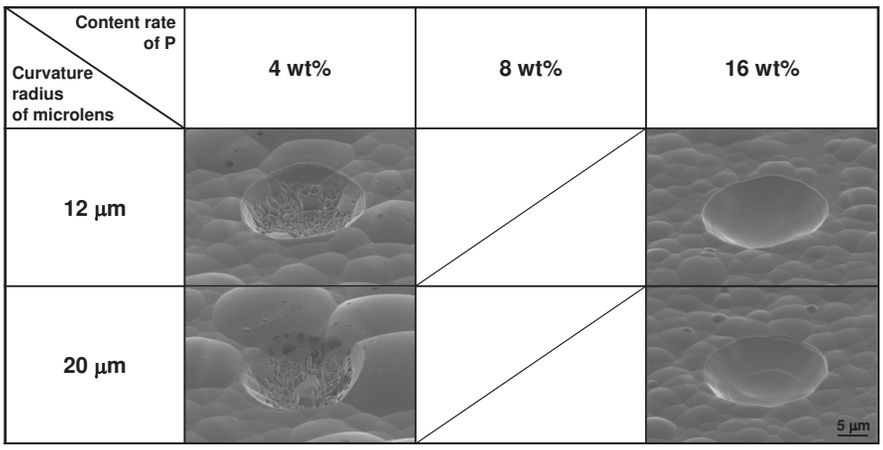

Figure 13. SEM images of microlens patterns on Ni-P alloy mold using unpolished Inconel-600 substrates.

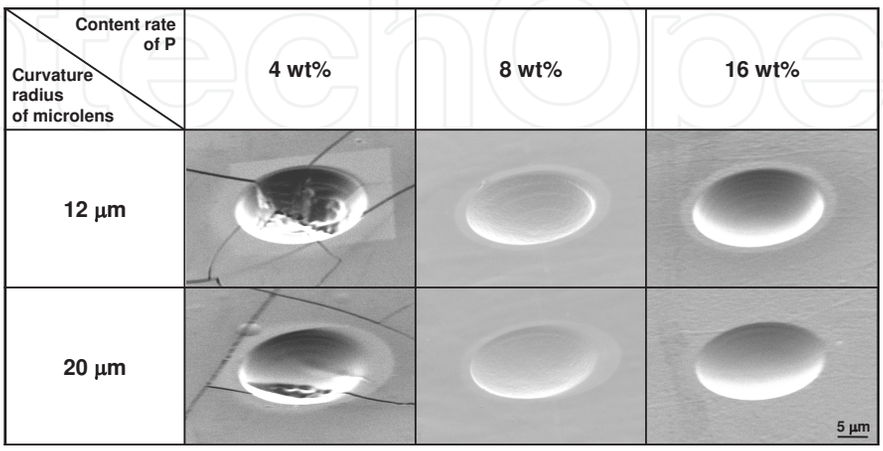

Figure 14. SEM images of microlens patterns on Ni-P alloy mold using polished Inconel-600 substrates.

http://dx.doi.org/10.5772/60408

4.1.3. Thermal treatment

To improve the hardness of the mold, an amorphous Ni-P alloy after FIB etching was thermally treated at 400 ºC for 3 h using the same system ASHE0201. Normally, the heating temperature to imprint on Pyrex glass is 600-650 ºC. Therefore, after a thermal treatment at 400 ºC, the substrate was heated at 600 or 650 ºC for 10 min. An Inconel-600 substrate was also thermal-treated under the same conditions for comparison.

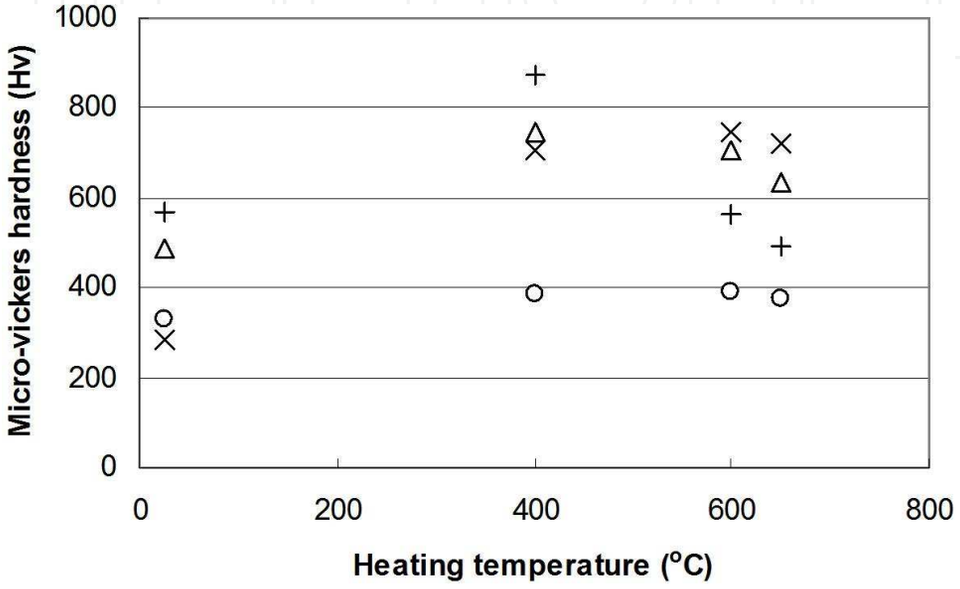

Figure 15. Relation between the heating temperature and the micro-vickers hardness of electroless-plated Ni-P alloys and the Inconel-600 substrate.

Figure 15 shows the results of measuring the micro-vickers hardness of these substrates with a micro-vickers hardness tester Matsuzawa MMT-X3. The micro-vickers hardness of the amorphous Ni-8P alloy increased to Vicker's hardness HV = 850 by thermal treatment at 400 ºC. Even if Ni-4P and Ni-16P substrates were heated to 600 ºC or more, the rate of the hardness decrease seemed to be gradual (comparatively speaking). In the case of the Inconel-600 substrate on which a Ni-P layer was not plated, the thermal treatment temperature influence on micro-vickers hardness was minor. Stiffening started by a precipitation of Ni_3P when the Ni-P alloy was heated at 400 ºC or higher. However, softening of the Ni-P alloy started by heating it at temperatures higher than 450 ºC, which is also the temperature at which micro-vickers hardness approaches the value of the Ni_3P crystal [11]. On the other hand, it hardly changes for Inconel-600 and maintains a value lower than HV of 400. This phenomenon can be confirmed from the results of the X-ray diffraction spectrum measured with MXP18AV (Bruker AXS) as shown in Fig. 16. The peaks of Ni(111), Ni(200), Ni(220), and Ni(311) that show crystalline states of Ni can be confirmed in a pure Ni substrate. In the amorphous Ni-P alloy substrate, a clear peak was not seen before thermal treatment at 400 ºC; and the entire spectrum appeared as broad as in an amorphous material. In Ni-4P and Ni-16P alloys thermally treated at 400 ºC for 3 h, a new peak did not appear. On the other hand, after the Ni-8P alloy was

thermally treated for 3 h at 400 ºC, new peaks of $Ni_3P(031)$, $Ni_3P(231)$, and $Ni_3P(141)$ that originated in Ni_3P in addition to the peaks of Ni(111), Ni(200), and Ni(220) were seen. In the case of the Ni-8P alloy thermally treated at 400 ºC for 3 h, the alloy developed a crystalline form in which its micro-vickers hardness decreased abruptly. A rise in the hardness resulted in a phase change from an amorphous phase into a meta-stable crystal phase when the amorphous Ni-P alloys were thermally treated at 400 ºC. In addition, the hardness reaches a maximum when the sample changes into Ni_3P and Ni with a highly crystalline structure. Thus, it is necessary to thermally treat the amorphous Ni-P alloy mold at 400 ºC to increase its mechanical strength, and to improve its thermal tolerance at high temperatures. After a thermal treatment at 400 ºC for 3 h, Ni-P alloys were heated to 600 or 650 ºC for 10 min, and the peaks originating in the crystal of Ni_3P and Ni were observed in all substrates. The crystallization of Ni_3P and Ni progressed when the Ni-P alloys were heated to 450 ºC or more. Moreover, when Ni-P alloys were heated to 600 or 650 ºC, many fine particles precipitated in the crystal [11]. The Ni-P alloy, in which a crystal grain boundary exists, became fragile. The reason for this is a decrease in the micro-vickers hardness mentioned earlier.

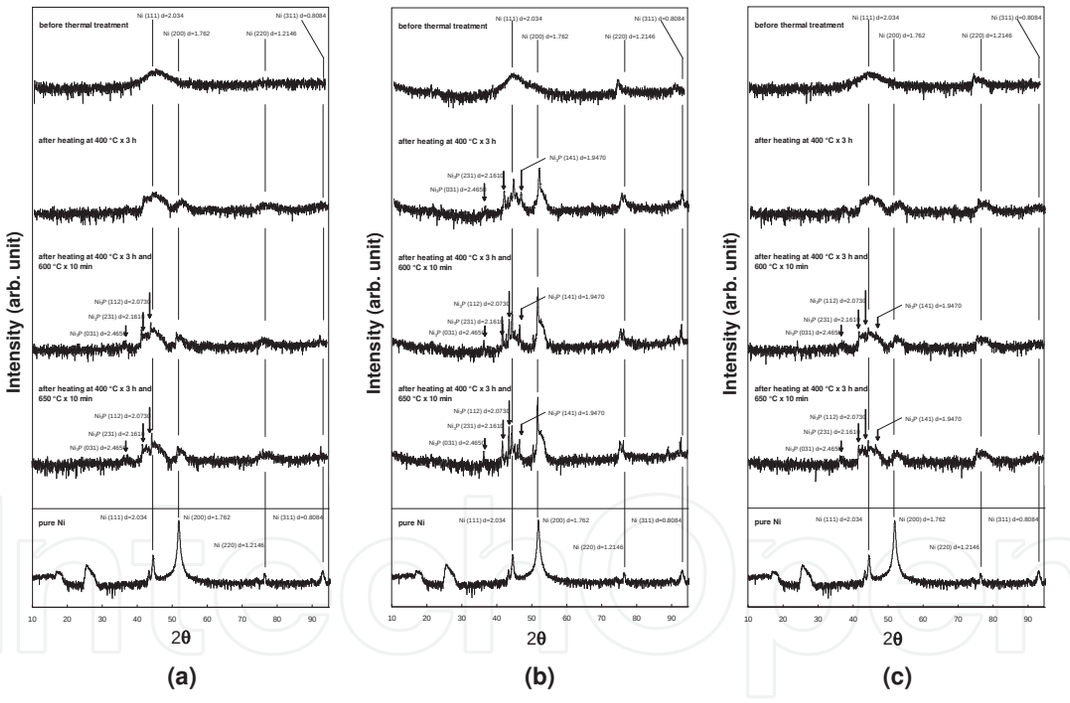

Figure 16. X-ray diffraction spectra of electroplated pure Ni and (a) electroless-plated Ni-4P alloy, (b) electroless-plated Ni-8P alloy, and (c) electroless-plated Ni-16P alloy.

4.2. Thermal imprint on Pyrex glass

The high-temperature thermal nanoimprint system, ASHE0201, was used for the thermal imprint experiment on Pyrex glass. When the temperature reached the set value, a contact force of 400 N was applied and maintained for a fixed time. Afterwards, the cooling process

http://dx.doi.org/10.5772/60408

was started, and we waited for the amorphous Ni-P alloy mold and Pyrex glass to cool down to 200 ºC in the vacuum for about 1 h. In the imprinting process, we experimented at heating temperatures of 630 and 640ºC and changed the contact times to 10 and 20 min. As mentioned previously, a thermal-treatment process was executed without applying a loading force according to a similar procedure with the same system as in the thermal imprint experiment.

4.3. Experimental results and discussion

4.3.1. SEM Observation

Figure 17 shows the SEM images of the microlenses imprinted on Pyrex glass using Ni-4P and Ni-16P/unpolished-Inconel-600 molds. The heating temperature was 640 ºC and the contact time was 20 min for these experimental conditions. Surface roughness is a critical factor in the fabrication of microlenses. When unpolished Inconel-600 molds were used, the processing accuracy was low. The irregularity of the surface of Ni-P/unpolished-Inconel-600 molds was transcribed on Pyrex glass because of the influence of the surface roughness. On the other hand, when imprinting with the Ni-P/polished-Inconel-600 molds under the same conditions as with the unpolished Inconel-600 molds, the surface of the mold patterns and imprinted Pyrex glass lenses were very smooth, as shown in Fig. 18; and the difference from Ni-P/unpolished-Inconel-600 mold seemed remarkably clear. However, it was observed that the imprinted patterns were bulldozed sideways. The deformed pattern appeared to be pushed aside considerably when the Ni-8P/polished-Inconel-600 mold was used. The width of the deformation was not large, although a similar phenomenon was seen when the Ni-16P/polished-Inconel-600 mold was used. Imprinting using the Ni-16P/polished-Inconel-600 mold resulted in almost complete microlenses being processed. The heights of the microlenses imprinted under the four molding conditions were measured by a 3D optical profiler, NewView 5000. The heating temperatures were 630 and 640 ºC. The contact time was changed to 10 or 20 min. Because the surface was very rough as shown in Fig. 17, the height could not be properly measured when imprinted using Ni-P/unpolished-Inconel-600 molds. Figure 19 shows the measured results of the Pyrex glass microlens with the curvature radius of 12 μm that was imprinted by using the Ni-P/polished-Inconel-600 molds. The maximum depths of the mold pattern on the Ni-4P, Ni-8P, and Ni-16P alloy molds were measured to be 4.4, 4.7, and 4.5 μm, respectively. The maximum heights of the imprinted microlenses were divided by the maximum depths of the corresponding mold pattern, and this value was defined as the filling rate. The filling rate rose when the heating temperature was 640 ºC, regardless of which mold was used; and lengthening of the contact time also produced a higher filling rate. It became clear that heating temperature was a more effective parameter to raise the filling rate than the contact time was. The same tendency was observed for microlenses with a curvature radius of 20 μm as shown in Fig. 20. The maximum depths of the mold pattern of Ni-4P, Ni-8P, and Ni-16P alloy molds were measured to be 2.4, 2.3, and 2.2 μm, respectively. The filling rate rose, although the maximum depth of the mold patterns decreased compared with the microlenses with a curvature radius of 12 μm. When the heating temperature and the contact time were 640 ºC and 20 min, the filling rate was close to 1 for every mold.

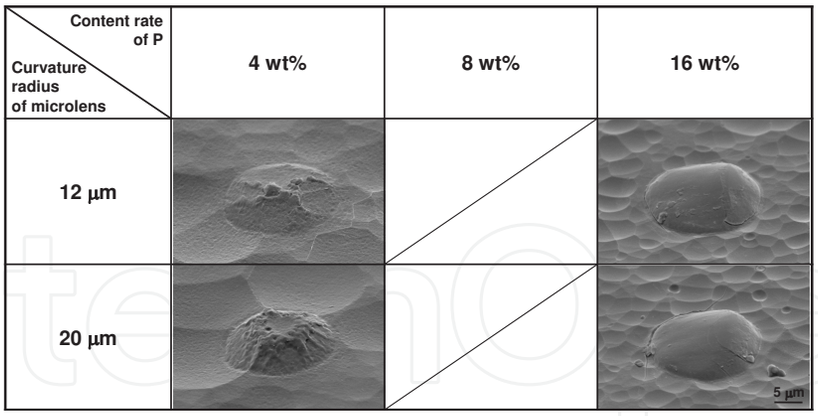

Figure 17. SEM images of microlenses on Pyrex glass using Ni-P/unpolished-Inconel-600 mold.

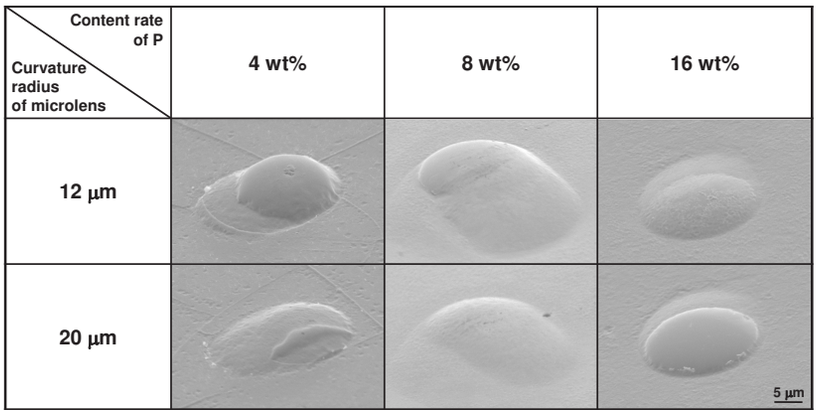

Figure 18. SEM images of microlenses on Pyrex glass using Ni-P/polished-Inconel-600 mold.

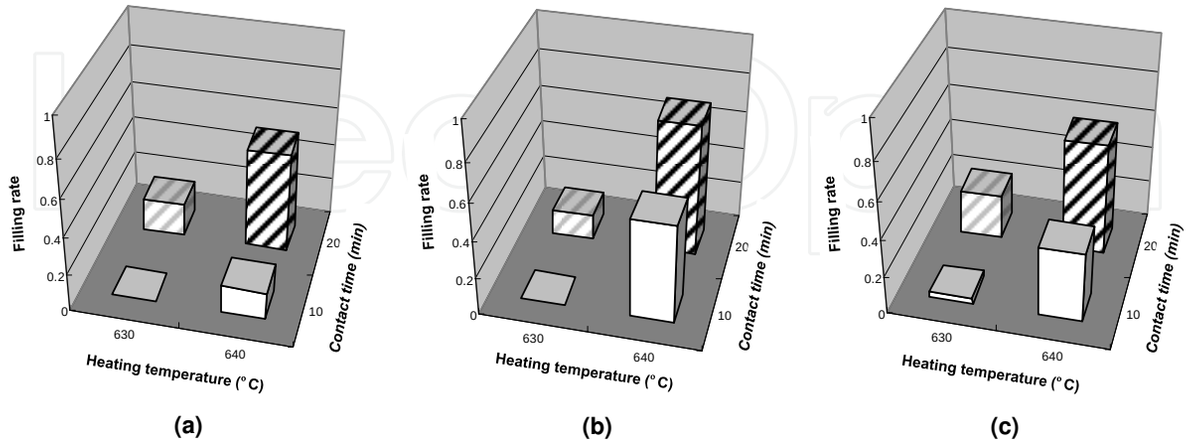

Figure 19. Filling rate of Pyrex glass into microlens patterns with a curvature radius of 12 μm when heating temperature and contact time were changed. The molds used in the imprint process were: (a) Ni-4P/polished-Inconel-600 mold, (b) Ni-8P/polished-Inconel-600 mold, and (c) Ni-16P/polished-Inconel-600 mold.

http://dx.doi.org/10.5772/60408

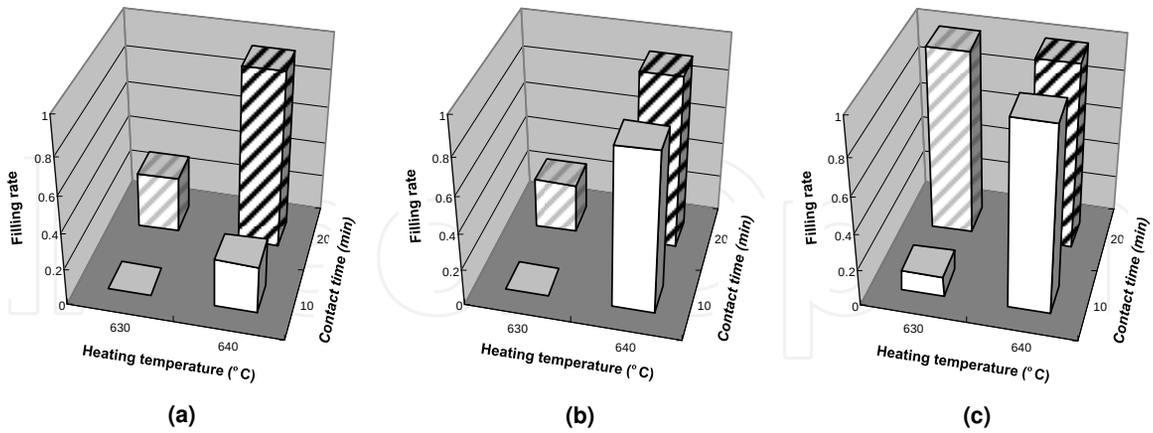

Figure 20. Filling rate of Pyrex glass to microlens patterns with a curvature radius of 20 μm when heating temperature and contact time were changed. The molds used in the imprint process were: (a) Ni–4P/polished-Inconel-600 mold, (b) Ni–8P/polished-Inconel-600 mold, and (c) Ni–16P/polished-Inconel-600 mold.

4.3.2. Profile measurement

The e-beam 3D surface roughness analyzer (ERA-8900) [23] developed by Elionix Inc. was used to evaluate the shape of the microlens. In general, the contrast in the SEM image originates from roughness on the surface of the sample and corresponds to the number of the secondary electrons detected with a second electronic detector. The amount of generation of the secondary electron depends on the angle of the gradient on the surface of the sample and increases linearly between 0 and 75⁰. Four additional electronic detectors were installed in this device, where a precise roughness and gradual undulation can be observed. It is possible to draw a 3D profile in an arbitrary place based upon the SEM image associated with a high-resolution evaluation [23]. Figure 21 shows cross-sectional profiles of the microlenses measured using ERA-8900. Figures 21(a)–21(c) show the profiles of the microlenses with a curvature radius of 12 μm, and Figs. 21(d)–21(f) show those of microlenses with a curvature radius of 20 μm. In the left, centre, and right figures, the molds used to imprint Pyrex glass were Ni-4P, Ni-8P, and Ni-16P/polished-Inconel-600 molds. Patterns imprinted at a heating temperature of 640 ⁰C for 20 min resulted in the observation of the highest filling rate. The original mold pattern is concave. However, the profile of the mold pattern shown by "x" marks in the figures was reversed in the vertical and horizontal orientations, and plotted as a convex shape. Moreover, the dotted lines in the figure are the profiles of the designed microlenses. In the case of a curvature radius of 12 μm, softened Pyrex glass was not completely filled into the mold pattern. This fact can be confirmed even at the low filling rate in Fig. 19. It is believed that the mold pattern was destroyed by the softened Pyrex glass before filling, and the entrance of the mold pattern was forcefully expanded outward. On the other hand, when the curvature radius was 20 μm, the depth of the mold pattern was shallow. In the case of either a 12 or a 20 μm curvature radius, the profile of the mold patterns and the microlenses correspond well. Therefore, it can be said that the transcript was well executed. The effect of the content ratio of P on the transcript was not particularly noticeable.

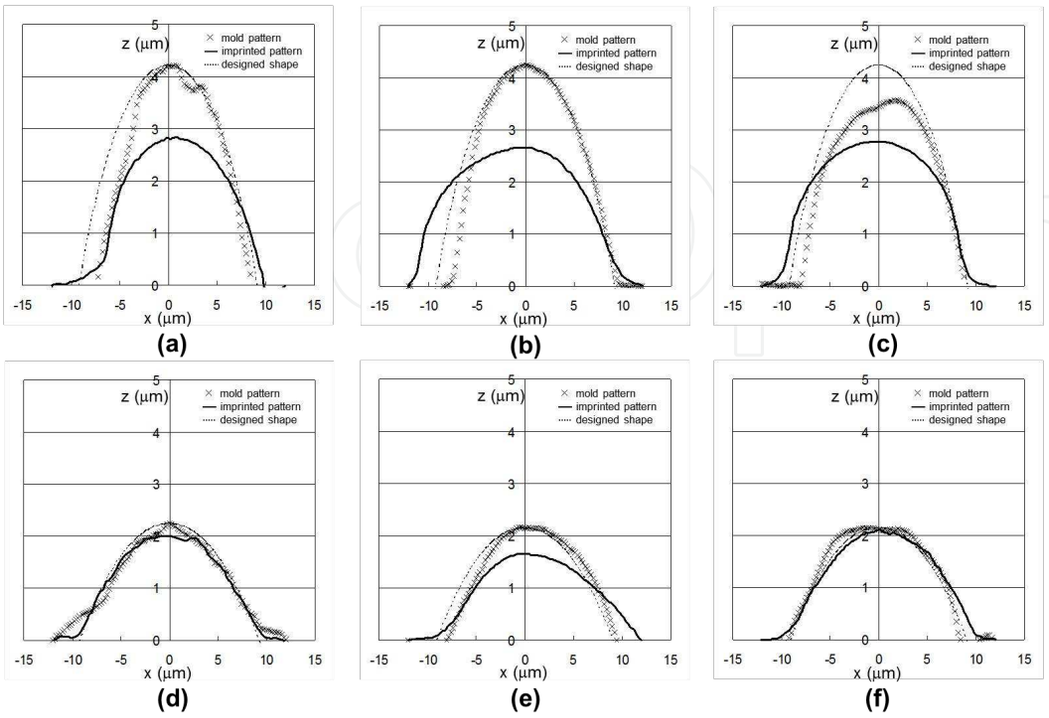

Figure 21. Measured cross-sectional profile of: (a) Ni–4P/polished-Inconel-600 mold and Pyrex glass microlens with a curvature radius of 12 μm, (b) Ni–8P/polished-Inconel-600 mold and Pyrex glass microlens with a curvature radius of 12 μm, (c) Ni–16P/polished-Inconel-600 mold and Pyrex glass microlens with a curvature radius of 12 μm, (d) Ni–4P/polished-Inconel-600 mold and Pyrex glass microlens with a curvature radius of 20 μm, (e) Ni–8P/polished-Inconel-600 mold and Pyrex glass microlens with a curvature radius of 20 μm, and (f) Ni–16P/polished-Inconel-600 mold and Pyrex glass microlens with a curvature radius 20 μm.

4.4. Application to large-area imprinting

Lastly, we report the results of imprinting a pattern that is larger than the microlenses on Pyrex glass. The pattern shape was an AIST logo of two different sizes. The size of the large logo pattern was about 250 x 50 mm^2, and for the small logo, the pattern was about 125 x 25 mm^2; a 50% reduction was also applied to other features in the vicinity. Figure 22(a) is an SEM image of a Ni-16P/unpolished-Inconel-600 mold, and Fig. 22(b) is that of a Ni–16P/polished-Inconel-600 mold. Figure 22(c) is the result of imprinting on Pyrex glass using the Ni-16P/unpolished-Inconel-600 mold. Regarding the molding conditions, the heating temperature, the contact time, and the loading force were kept at 640 ^{0}C, 20 min, and 700 N, respectively. In regard to the width, the character "I" in the large AIST logo pattern was measured. The width of the mold pattern was measured to be 8.3 μm, and the width of the imprinted pattern was also measured to be 8.3 μm. In the case of the small logo pattern, the width of the mold pattern was 4.5 μm, and the width of the imprinted pattern was 4.4 μm, which was almost same, considering the margin of error. On the other hand, Fig. 22(d) is an SEM image of the logo pattern when Pyrex glass was imprinted using the Ni-16P/polished-Inconel-600 mold. The surface of

http://dx.doi.org/10.5772/60408

the pattern appeared very smooth. When the width of the logo was measured, there was a difference between Figs. 22(b) and 22(d). The width of the imprinted pattern was 9.5 μm, while the width of the mold pattern was 8.7 μm in the case of the large logo. Moreover, with respect to the small logo pattern, the 4.9-μm-wide mold pattern was transcribed to the imprinted pattern at a width of 6.3 μm. In terms of a more comprehensive observation, the Ni-16P/unpolished-Inconel-600 mold seemed to be transcribed faithfully according to the pattern size. However, the surface of the imprinted patterns is quite different as is the microlens formation. Figure 23 shows expanded SEM images of a small AIST logo when observed at an inclined angle of 60^0. It is clear that the surface roughness of the molds influenced the imprinting accuracy. It seems to be important in precise Pyrex glass imprinting to add a polishing process to the Inconel-600 substrate by CMP technologies. When modifying one's views, for large irregularities on the surface of the Ni-16P/unpolished-Inconel-600 mold, it is assumed that the mold and the Pyrex glass are firmly fixed by an anchoring force, and that the extra flow of the softened Pyrex glass is suppressed. The depth of the mold pattern on the Ni-16P/polished-Inconel-600 mold measured with the NewView 5000 was 1.1 μm, and the height of the AIST logo imprinted on the Pyrex glass was 0.94 μm.

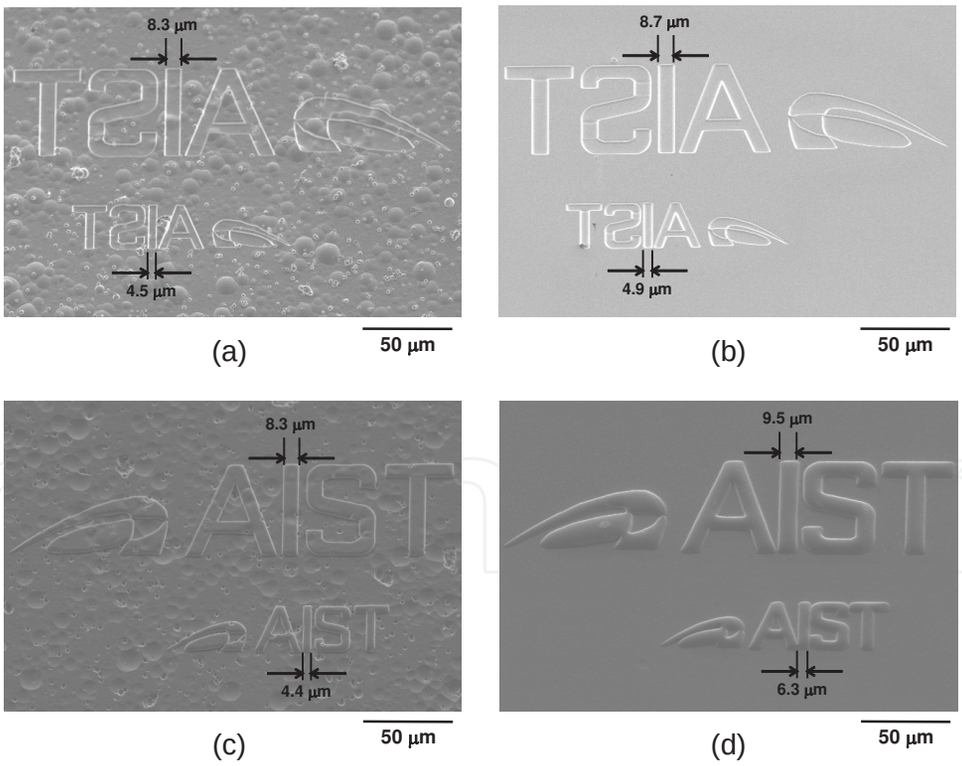

Figure 22. SEM images of AIST logo patterns on: (a) Ni-16P/unpolished-Inconel-600 mold, (b) Ni-16P/polished-Inconel-600 mold, (c) Pyrex glass imprinted using Ni-16P/unpolished-Inconel-600 mold, and (d) Pyrex glass imprinted using Ni-16P/polished-Inconel-600 mold.

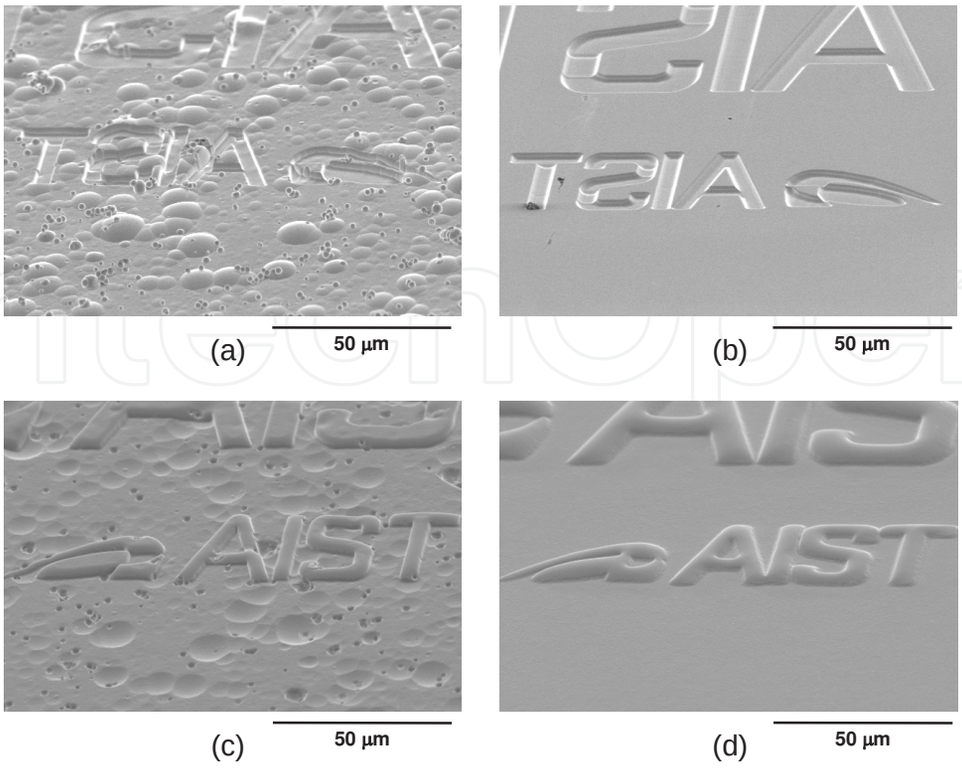

Figure 23. Expanded SEM images of the small AIST logo pattern from Fig. 22 when observed at an inclined angle of 60^0.

5. Conclusions

At first, the author experimentally confirmed that an amorphous Ni–P alloy can be used as a mold material for nanoimprint lithography of Pyrex glass. Using X-ray diffraction, it was established that a P content of 8 wt.% was the right amount to make Ni an amorphous material. Moreover, it was shown that in fabricating the nanopatterns using FIB, and by making the Ni-P alloy amorphous it was possible to prevent the deterioration of process accuracy caused by the existence of crystal granularity. In addition, the hardness of the amorphous Ni-P alloy was rapidly improved by thermal treatment at 400 °C, which succeeded in creating characteristics more suitable for a mold material. And moreover, the author experimented with nanoimprint lithography using Pyrex glass and succeeded in molding patterns with linewidths of as little as 500 nm.

Next, the author improved and perfected a low-cost high-accuracy mold for Pyrex glass imprinting. In this process, an amorphous Ni-P plating layer was deposited on a Ni/Ti/Si substrate by electroless-plating, and then a microlens pattern was created on the surface by using an FIB system equipped with a 3D-CAD software. Compared to pure Ni mold, the amorphous Ni-P mold showed a superior processing accuracy by FIB. Especially, in the case

http://dx.doi.org/10.5772/60408

of large microlens with a curvature radius of 20 μm where amorphous Ni-P alloy mold was not used, an imprinted pattern could not be observed on a Pyrex glass. The Ni-P/Ni/Ti/Si mold could be heated up to 620 ºC, whereas the Ni-P/Cu/Cr/Si mold could not be used at this high temperature.

Finally, the author successfuly completed a low-cost high-accuracy mold for imprinting Pyrex glass. A plating layer of amorphous Ni-P was formed on an Inconel-600 substrate by an electroless-plating technique, and on which a microlens patterns were formed with a FIB system equipped with a 3D-CAD software. The author learned that the hardness of a Ni-P layer can be increased by subjecting it to a thermal treatment at 400 ºC for 3 h. Experiments were carried out to compare the impacts of polished and unpolished surfaces of Inconel-600 substrates prior to electroplating Ni-P layers. It was found to be very important to have a smooth surface on the Pyrex glass and to add this requirement to the process whereby the surface of the substrate was polished before Ni-P electroless-plating. In addition, the content ratio of P = 16 wt.% seemed to be more suitable than of P = 4 wt.% or P = 8 wt.% for achieving high hardness after the thermal treatment, and for obtaining smoothness over the rough surface of the mold. Moreover, raising the heating temperature improved the molding accuracy in the imprint process on Pyrex glass more than could be achieved by simply extending the contact time. Finally, microlenses with a 20 μm radius of curvature; and an AIST logo with a character width of 10 μm (or less) were successfully imprinted on Pyrex glass. We also proved experimentally that a Ni-P alloy can be used as a mold material to imprint on Pyrex glass at high temperature around 640 ºC.

Acknowledgements

The electroplated pure Ni and Ni-P substrates were supplied by Dr. Manabu Yasui of Kanagawa Industrial Technology Center and Takeshi Kitadani of Sawa Plating Co., Ltd, respectively. The author received valuable technical support from Chieko Okuyama of National Institute of Advanced Industrial Science and Technology and Michiru Yamashita of Hyogo Prefectural Institute of Technology. For FIB etching and e-beam 3D surface roughness analysis the author received technical supports from Tomoyuki Tsuchida and Dr. Jun-ichi Uegaki of Elionix Inc. The author thanks them for their advice and cooperation.

Author details

Harutaka Mekaru*

Address all correspondence to: h-mekaru@aist.go.jp

National Institute of Advanced Industrial Science and Technology (AIST), Tokyo, Japan

References

[1] Chou SY, Krauss PR, Renstrom PJ. Imprint of sub-25 nm vias and trenches in polymers. Applied. Physics Letter. 1995; 67(21) 3114-3116.

[2] Haisma J, Verheijen M, van den Heuvel K, van den Berg J. Mold-assisted nanolithography: A process for reliable pattern replication. Journal of Vacuum Science and Technology. B 1996; 14(6) 4124-4128.

[3] Colburn M, Johnson SC, Stewart MD, Damle S, Bailey TC, Choi B, Wedlake M, Michaelson T, Sreenivasan SV, Ekerdt J, Wilson CG. Step and flash imprint lithography: a new approach to high-resolution patterning: proceedings of the International Society for Optics and Photonics: Vladimirsky Y. (ed.) Emerging Lithographic Technologies III, 15-17 March 1999, Santa Clara, California: the International Society for Optics and Photonics; 1999; 3676 379-390.

[4] Sotomayor Torres CM. Alternative Lithography: Unleashing the Potentials of Nanotechnology. New York: Kluwere Academic/Plenum Pubkishers; 2003.

[5] Takahashi M, Sugimoto K, Maeda R. Nanoimprint of Glass Materials with Glassy Carbon Molds Fabricated by Focused-Ion-Beam Etching. Japanese Journal of Applied Physics Part 1. 2005; 44(7B) 5600-5605.

[6] Mekaru H, Okuyama C, Ueno A, Takahashi M. Thermal imprinting on quartz fiber using glasslike carbon mold. Journal of Vacuum Science and Technology B. 2009; 27(6) 2820-2825.

[7] Takahashi M, Maeda R. Large-Area Micro-Hot.Embossing of Glass Materials with Glassy Carbon Mold Machined by Dicing. Journal of the Japan Society for Technology of Plasticity. 2006; 47(549) 963-967 [in Japanese].

[8] Takahashi M, Goto H, Maeda R, Maruyama O. Desktop Nanoimprint System –Prototype and Performance: proceedings of the Japan Society for Precision Engineering Conference. 15-17 March 2006, Noda, Chiba: the Japan Society for Precision Engineering ;2006; 737-738 [in Japanese].

[9] Ikeda K. Bisai Tensha: Kako Gijutsu Zenshu (The Complete Works of Precise Transfer and Processing Technology). Tokyo: Technical Information Institute; 2008 [in Japanese].

[10] Takahashi M, Maeda R. Sugimoto K. Micro/nano-Hot Embossing of Quartz Glass Materials with Glassy Carbon Mold Prepared by Focused Ion Beam. Journal of the Japan Society for Technology of Plasticity. 2006; 47(549) 958-962 [in Japanese].

[11] Masui K, Maruno S, Yamada T. Heat-Induced Structural Changes in Electrodeposited Ni-P Alloys. Journal of the Japan Institute of Metals and Materials. 1977; 41 1130-1136 [in Japanese].

[12] Hou K, Jeng M, Ger M. A study on the wear resistance characteristics of pulse electroforming Ni-P alloy coatings as plated. Were. 2007; 262(7-8) 833-844.

[13] Yasui M, Takahashi M, Kaneko S, Tsuchida T, Hirabayashi Y, Sugimoto K, Uegaki J, Maeda R. Micro Press Molding of Borosllicate Glass Using Plated Ni-W Molds. Japanese Journal of Applied Physics Part 1. 2007; 46(9B) 6378-6381.

[14] Inoue A, Takeuchi A. Recent Progress in Bulk Glassy Alloys. Materials Transactions. 2002; 43(8) 1892-1906.

[15] Takenaka K, Togashi N, Nishiyama N, Inoue A. Structure, mechanical properties and imprint-ability of Pd-Cu-Ni-P glassy alloy thin film prepared by a pulsed-laser deposition method. Journal of Non-Crystalline Solids. 2010; 356(31-32) 1542-1545.

[16] Wheeler JM, Raghavan R, Michler J. *In situ* SEM indentation of a Zr-based bulk metallic glass at elevated temperatures. Materials Science and Engineering A. 2011; 528(29-30) 8750-8756.

[17] Tan H, Gildertson A, Chou SY. Roller nanoimprint lithography. Journal of Vacuum Science and Technology B. 1998; 16(6) 3926-3928.

[18] Morikawa T, Yokoi M, Eguchi S. Amorphous plating and the applications of this. Science and Industry. 1991; 41 213-221 [in Japanese].

[19] Mekaru H, Kitadani T, Yamashita M, Takahashi M. Glass nanoimprint using amorphous Ni-P mold etched by focused-ion beam. Journal of Vacuum Science and Technology A. 2007; 25(4) 1025-1028.

[20] Mekaru H, Tsuchida T, Uegaki J, M, Yasui M, Yamashita M, Takahashi M. Micro lens imprinted on Pyrex glass by using amorphous Ni-P alloy mold. Microelectronic Engineering. 2008; 85 873-876.

[21] Katayama K. The Japan Society of Mechanical Engineering Data Book Heat Transfer 4th Ed. Tokyo: the Japan Society of Mechanical Engineers; 1986 [in Japanese].

[22] INCONEL alloy 600. Huntington: Special Metals Corporation. SMC-027; 2008.

[23] Taguchi Y, Omata Y. Electrodeposition of the Composite Film of Nickel and Hydrophobic Graphite Particles. Journal of the Surface Finishing Society of Japan. 2006; 57(8) 564-583 [in Japanese].

[24] Mekaru H, Okuyama C, Tsuchida T, Yasui M, Kitadani T, Yamashita M, Uegaki J, Takahashi M. Development of Ni-P-Plated Inconel Alloy Mold for Imprinting on Pyrex Glass. Japanese Journal of Applied Physics. 2009; 48 06FH06-1-06FH06-10.

IntechOpen